Supplement of Atmos. Chem. Phys., 22, 3525–3533, 2022
https://doi.org/10.5194/acp-22-3525-2022-supplement

Atmospheric Chemistry and Physics Open Access

Supplement of

Interpretation of NO_3–N_2O_5 observation via steady state in high-aerosol air mass: the impact of equilibrium coefficient in ambient conditions

Xiaorui Chen et al.

Correspondence to: Haichao Wang (wanghch27@mail.sysu.edu.cn) and Keding Lu (k.lu@pku.edu.cn)

Contents

S1. Ambient case invalid for NO_3-N_2O_5 steady state analysis

Take two typical cases in winter and summer respectively for example to illustrate the conditions under which steady state analysis is invalid for interpreting NO_3-N_2O_5 observation and deriving $\gamma(N_2O_5)$. Over the period of wintertime case shown in Figure S1, the NOx and Sa concentration were low, indicating a clean episode. The $\gamma(N_2O_5)$ and $k NO_3$ can be determined from the intercept and slope respectively by linear fit based on steady state equation Eq. (5). The details and derivation of this approach are provided in introduction and method section. Albeit the correlation coefficient for deriving $\gamma(N_2O_5)$ by steady state approximation appears to be high, an unreasonably negative $k NO_3$ value derived during this analysis period (Figure S1d) indicates that the steady state in this case still requires much longer induction time due to low strength of NO_3-N_2O_5 sink. In summertime case, although large sink rate contributed to fast approach of steady state, frequent injection of NOx emission could significantly modify the air mass condition. The time for mixing and reacting was still less than enough as emissions deviates the air mass from steady state (Figure S1e-S1g), leading to weak correlation factors (Figure S1h).

S2. Observation datasets from field campaigns 2017PKU and 2018TZ

The datasets used for analysis in this study were obtained from two field campaigns with different ambient conditions. The PKU2017 winter campaign took place from mid-November to late-December 2017 in the campus of Peking University, which is at urban area of Beijing, China. And the other one TZ2018 summer campaign took place from late-May to mid-June 2018 at a suburban supersite, Taizhou, China. More specific information about these two campaigns can be referred to our previous studies (Ma et al., 2019;Wang et al., 2020), while only basic background of site location and analysis-relevant instrumentation are provided below.

During the PKU2017 campaign, all instruments were applied on the roof of building in the campus of Peking University, which was about 100 m west to the major roads with strong influence of vehicle emissions. Each sampling inlet was distributed at least 20 m above the ground. The strong northerly winds with dry and clean air mass during the winter would periodically transport to this site, bring in fresh O_3 at night. The TZ2018 site is surrounded by agricultural land and fishponds, resulted in strong influence of biogenic emissions and occasional biomass burning. Each sampling inlet was distributed about 5 m above the ground. It should be noted that low concentration level of NO was frequently observed at this site due to a major highway within 0.5 km.

Same instrumentation was implemented in these two campaigns, and the related information are given in Table S1. We adjusted the nighttime NO concentration near the detection limit to zero during the periods with O3 concentration higher than 25 ppbv, as the lifetime of NO would be extremely short at night under this condition and the NO measurement at the low level usually has large uncertainty.

S3. Characteristic of nighttime NO_3-N_2O_5 loss pathway in half-artificial dataset

The validity of NO_3-N_2O_5 steady state depends on their atmospheric lifetime, in other words their loss rate constants (Brown et al., 2003). In different seasons or areas, variations of emission, temperature, and other relevant factors can sufficiently change the sink strength of ambient NO_3 and N_2O_5 and thus relative occupations of these pathways. As half-artificial datasets (detailed in Methods) indicated, the average nighttime loss rate of NO_3 and N_2O_5 at PKU site in winter were 41 pptv h^{-1} and 195 pptv h^{-1}, whereas much higher rates were obtained at TZ2018 campaign with 451 pptv h^{-1} for NO_3 and 390 pptv h^{-1} for N_2O_5. Distinguished from a dominant sink rate of N_2O_5 in winter, total sink rate attribution shifted to NO_3 side in summer with significant larger sink strength than that in winter. The average proportions of NO_3 and N_2O_5 removal in each night is shown in Figure S2, where the nights with missing data represents that there is less than 15% valid data. Under the condition of approximate steady state, the sink flux contributed through N_2O_5 reaches up to 55~95% in wintertime campaign 2017PKU with an average higher than 80%, whilst it turns out to be less than 50%, even 5%, in 2018TZ summer campaign. Besides the different emission compositions at these two sites leading to significant distinction of removal attribution (strong biogenic emission at TZ site and high anthropogenic emission at PKU site), high temperature during summer facilitates the equilibrium in reactions R1 shifting to NO_3, further increasing the sink flux of NO_3. The attribution of removal pathways among NO_3 and N_2O_5 directly determines the weights of two terms on the right side of steady state expressions Eq. (4) and Eq. (5), contributing to assessing the impacts of several variables on steady state fitting among different reactivity conditions.

Taking two typical cases from these two datasets for example, the N_2O_5 lifetime was about 20 minutes in winter (Figure S3(a)), while was largely reduced to 100 seconds for summertime case (Figure S3(c)). The steady state lifetime of N_2O_5 ($\tau_{ss}(\mathrm{N_2O_5}) = \frac{[\mathrm{N_2O_5}]}{k_{\mathrm{R1}}[\mathrm{NO_2}][\mathrm{O_3}]}$) and calculated lifetime of N_2O_5 ($\tau_{calc}(\mathrm{N_2O_5}) = (k_{N_2O_5} + \frac{k_{NO_3}}{K_{eq}[\mathrm{NO_2}]})^{-1}$) were used for determine whether the situation had satisfied steady state (see details in methods section). Significantly different atmospheric lifetime for these two cases was majorly resulted from varying uptake

removal pathways instead of $k\mathrm{NO_3}$ from gas-phase reactions. Higher humidity at TZ site during nights facilitated hygroscopic growth of particles, the Sa concentration of which usually increased up to thousands of $\mu m^2\ cm^{-3}$ promoting the uptake reactions of NO_3 and N_2O_5, whereas Sa in the PKU site case become lower than 500 $\mu m^2\ cm^{-3}$ under the impact of clean and dry air mass. The steady state lifetime denoted by blue dash line in Figure S3(a)&(c), shows good agreement with atmospheric lifetime in both of cases, indicating that the NO_3-N_2O_5 chemical system simulated by steady state model is validated to be approximate steady state (deviation <5%). However, even in these cases, the derived uptake coefficient of N_2O_5, $\gamma_{ss}(N_2O_5)$, through steady state fitting (Figure S3(b)&(d)) still have a significant bias (>20%) from the setting values 0.02. Furthermore, we found that unexpected difference between $\gamma_{ss}(N_2O_5)$ fitting results and $\gamma(N_2O_5)$ setting values is common for all selected steady state periods in datasets. Since the influence of covariance of Sa and $K\mathrm{eq}\times[NO_2]$ has been avoided by applying Eq. (5) (Brown et al., 2009), the bias of $\gamma_{ss}(N_2O_5)$ presented in the above fitting calculation could be produced by interaction between equilibrium and steady state, variation of relevant parameters in the fitting equations (such as $k\mathrm{NO_3}$, $k\mathrm{N_2O_5}$, etc), which are discussed in the main text.

S4. Parameterization of *K*eq coefficient in different databases

*K*eq of NO_3-N_2O_5 system is a temperature dependent parameter, which has been extensively quantified in the laboratory (Pritchard, 1994). According to simultaneous measurements of N_2O_5, NO_3 and NO_2 concentration in a reaction chamber, the *K*eq can be directly calculated (Cantrell et al., 1988;Graham and Johnston, 1978;Osthoff et al., 2007), while the measurements of k_{R1a} and k_{R1b} or other accompanied parameters provides indirect ways to quantify *K*eq (Cantrell et al., 1993;Kircher et al., 1984;Smith and Ravishankara, 1985). However, distinct differences arise from these *K*eq results, which might be ascribed to the calibration uncertainty of absorption cross sections of NO_3 and NO_2 molecule (Osthoff et al., 2007). Jet Propulsion Laboratory (JPL) database provides an empirical formula, similar with Arenius formula, to calculate *K*eq in a simple way:

$$K_{eq}(JPL) = A \times \exp(B/T), \quad \text{(S1)}$$

Here T denotes ambient temperature, and coefficients A and B are empirical parameter derived from laboratory works. Nevertheless, only parameterizations of k_{R1a} and k_{R1b} based on fall-off curve are described in IUPAC database and most of chemical mechanisms, without a direct formula to estimate *K*eq value. To our best knowledge, only one previous study compared two of these parameterizations in terms of temperature dependence (Chang et al., 2011).

Here, a set of uniform formulas are applied to describing k_{R1a} and k_{R1b}, capable of reproducing the preferred values given by several popular atmospheric chemistry mechanisms (Mozart, CB05, Saprc07, RACM2 and kinetic databases JPL2015 as well as IUPAC2017) and finally calculating *K*eq. As shown in Eq. (S2) and Eq. (S3):

$$k_{R1a}([M], T) = \left(\frac{k_O(T)[M]}{1+\frac{k_O(T)[M]}{k_\infty(T)}}\right) \times F^{\left\{1+\left[\frac{log_{10}\left(\frac{k_O(T)[M]}{k_\infty(T)}\right)}{g}\right]^2\right\}^{-1}}, \quad \text{(S2)}$$

$$k_{R1b}([M],T) = \left(\frac{\frac{k_o(T)[M]e^{\frac{-B1}{T}}}{A}}{1+\frac{k_o(T)[M]e^{\frac{-B1}{T}}}{k_\infty(T)e^{\frac{-B2}{T}}}} \right) \times F^{\left\{ 1+\left[\frac{log_{10}\left(\frac{k_o(T)[M]e^{\frac{-B1}{T}}}{k_\infty(T)e^{\frac{-B2}{T}}} \right)}{g} \right]^2 \right\}^{-1}}, \quad \text{(S3)}$$

The parameter [M] represent molecular density in ambient air. $k_o(T)$ and $k_\infty(T)$ are rate coefficients of third-body reactions under low and high pressure respectively, which over different temperatures can be extrapolated by Eq. (S4) and Eq. (S5) based on 300 K measurement or simulation results:

$$k_o(T) = k_o^{300}\left(\frac{T}{300}\right)^{-n}, \quad \text{(S4)}$$

$$k_\infty(T) = k_\infty^{300}\left(\frac{T}{300}\right)^{-m}, \quad \text{(S5)}$$

All parameters in the above formulas are summarized in Table S3 and Table S4, which can be applied to calculating *K*eq coefficient via k_{R1a}/k_{R1b}. We found that there are significant differences among the parameters from these chemical mechanisms and databases, with a maximum discrepancy of 63% propagating to *K*eq at 298 K.

S5. Sensitivity tests of time to approach steady state

In Figure S8 and Figure S9, a series of sensitivity test provide an assessment of the time a valid steady state needs under several conditions. The most sensitive variables to the time to reach a valid steady state are $k_{N_2O_5}$, k_{NO_3} and T, the enhancement of which reduces the induction time, facilitating the approach to valid steady state of NO_3-N_2O_5 system. The time for a simulation of a particular case, starting from initialized conditions to meet the steady state criterion (detailed in the methods section), is defined as the time to reach a valid steady state. In the case of increasing $k_{N_2O_5}$ and k_{NO_3}, the fast approaching to stead state is accounted by lower concentration of NO_3 and N_2O_5 when the steady state is valid. By comparing the sensitivity tests based on summertime (Figure S8(a)) and wintertime (Figure S8(b)) conditions, the impacts of $k_{N_2O_5}$ on approaching steady state is found to be more efficient than that of k_{NO_3} in winter, while both contribute similarly in summer.

The different sensitivities to their reactivity in different seasons could be determined by the weights of loss pathways (Text S3). During the winter, such as the condition of PKU2017, the N_2O_5 usually accounted by over 80% of the overall loss frequency of NO_3-N_2O_5 system, leading to high sensitivity to $k_{N_2O_5}$, while comparable loss frequency was occupied by both of NO_3 and N_2O_5 during the summer. As for the temperature, lower temperature shifts the equilibrium in R1 to N_2O_5 side, which delay the time for developing equilibrium. By contrast, enhanced loss through NO_3 with higher ambient temperature decreases the influence of equilibrium, boosting the approach to steady state. Moreover, Figure S9 shows relatively weak sensitivity of NO_2 and O_3 concentration to steady state approach. While changing O_3 concentration barely contribute to promote a valid steady state in the scenario of this analysis, the NO_2 concentration shows a positive sensitivity in some cases. Like the ambient temperature, changing NO_2 concentration could shift the ratio of N_2O_5/NO_3 when steady state is valid and thus the time it requires. Especially under the condition of low ratio of NO_2 to O_3, like that in TZ2018, the enhancement of NO_2 concentration shift NO_3 to N_2O_5 production and amplify the influence of equilibrium reactions. Instead, with a sufficiently high ratio of NO_2/O_3, the loss associated with NO_3-N_2O_5 system has been already dominated by N_2O_5 removal,

164 eliminating the influence of NO_2 increase on delaying steady state. Previous research has also
165 found similar trends of time to develop steady state according to simple scenarios simulated
166 by box model (Brown et al., 2003).
167

S6. The impacts of $k\mathrm{NO_3}$ and $k\mathrm{N_2O_5}$ levels on $\gamma_{ss}(\mathrm{N_2O_5})$

In order to demonstrate the impacts of $k\mathrm{NO_3}$ level on deriving $\gamma_{ss}(\mathrm{N_2O_5})$, another three half artificial data set are formulated through steady state model also based on the same observational constraints with $k\mathrm{NO_3}$ levels increased to 3 times (Mod1), 6 times (Mod2) and 10 times (Mod3) respectively, while other parameters remained unchanged. Similarly, the steady state fitting is used to obtain $\gamma_{ss}(\mathrm{N_2O_5})$ for each 2-hour time-period as Mod0. The mean discrepancy from complete steady state of these time periods and the median deviation of derived $\gamma_{ss}(\mathrm{N_2O_5})$ from pre-set $\gamma(\mathrm{N_2O_5})$ are shown as solid circles and triangles in Figure S9. With the enhancement of $k\mathrm{NO_3}$ constraints, $\gamma_{ss}(\mathrm{N_2O_5})$ deviation from true value increase dramatically, though the $\mathrm{NO_3}$-$\mathrm{N_2O_5}$ system behave generally closer to steady state. A larger deviation of $\gamma_{ss}(\mathrm{N_2O_5})$ will be yielded from linear fit at a higher $k\mathrm{NO_3}$ level, while the relative varieties of $k\mathrm{NO_3}$ stay the same. It indicates that the region with strong biogenic emissions is not suited to steady state fitting, such as TZ site, neither are the time periods with NO injection due to the resulted high reactivity and fast variation. Therefore, air mass with medium to low level of $k\mathrm{NO_3}$ is required to produce accurate $\gamma_{ss}(\mathrm{N_2O_5})$ when applying stead state to analysis, like data sets of airborne or residual measurements (Brown et al., 2009;Brown et al., 2006;Morgan et al., 2015).

Similarly, the influence of different levels of $k\mathrm{N_2O_5}$ is also explored by adjusting the pre-set $\gamma(\mathrm{N_2O_5})$ or the Sa concentration constraint in the steady state model, as presented in the Figure S10(c)&(d). With the enhancement of $k\mathrm{N_2O_5}$ level up to 5 times (Mod4), 12.5 times (Mod5) and 25 times (Mod6) of that in Mod0, the steady state approach can provide more reliable results of $\gamma_{ss}(\mathrm{N_2O_5})$, especially in the summer data set. This is because a large $k\mathrm{N_2O_5}$ level contributes to approaching steady state, which instinctively attenuates the deviation of fitting results produced by the small difference between both sides of Eq. (5).

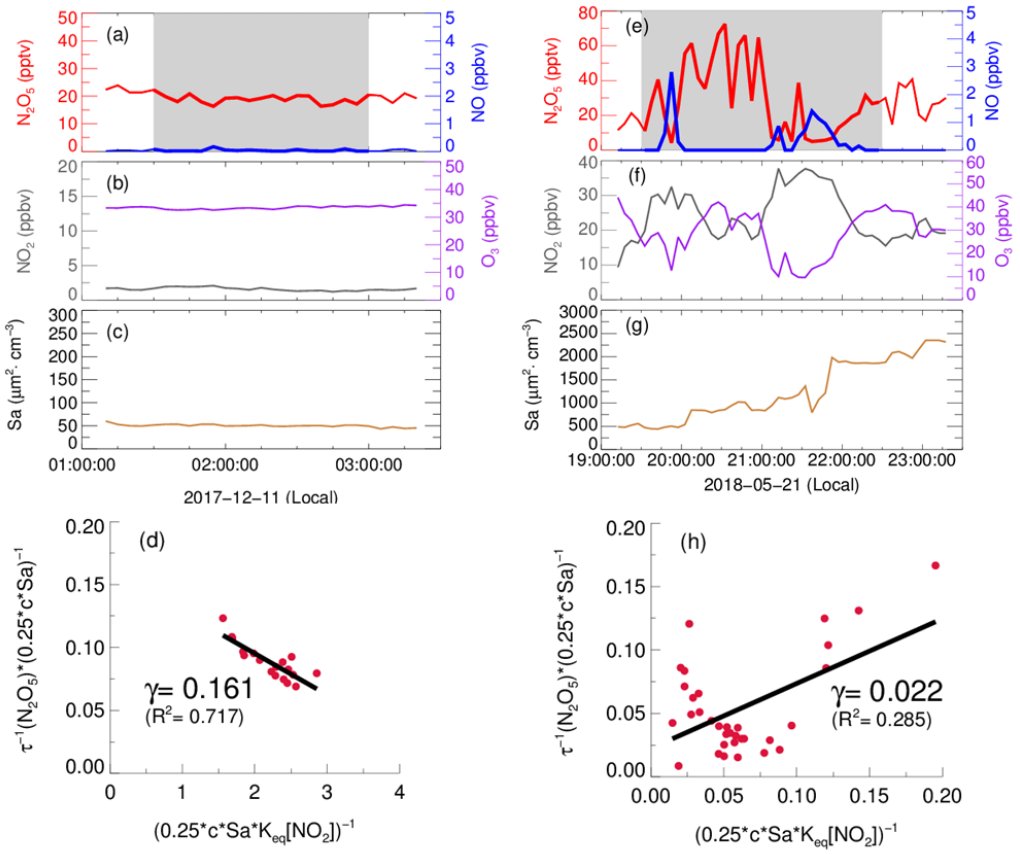

193

194 **Figure S1.** Exemplary steady state fit and the variations of relevant parameters in ambient conditions of
195 (a)&(b)&(c)&(d) PKU site and (e)&(f)&(g)&(h) TZ site. The red dots in (d)&(h) represent the correlation plot
196 between $\left(0.25cS_a\tau_{ss}(\mathrm{N_2O_5})\right)^{-1}$ and $\left(0.25cS_aK_{eq}[\mathrm{NO_2}]\right)^{-1}$ used for deriving $\gamma(\mathrm{N_2O_5})$ and $k\mathrm{NO_3}$ as illustrated
197 in the method. The text on the plot gives the best fit results of $\gamma(\mathrm{N_2O_5})$ and correlation coefficient.

198

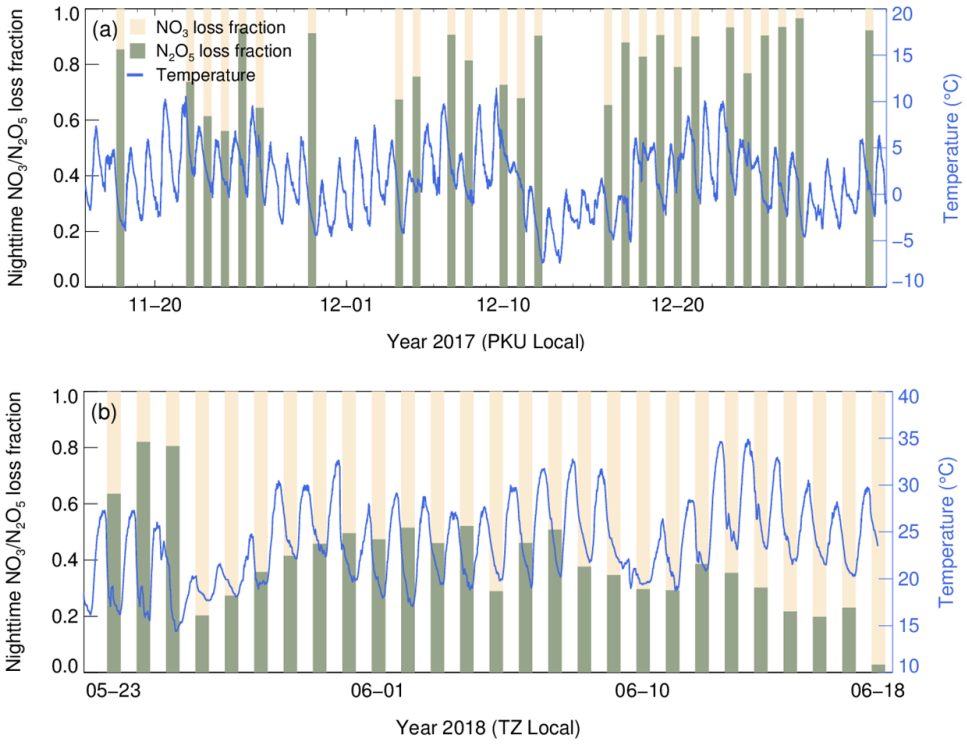

Figure S2. Timeseries of each night (SZA>90°) mean NO_3/N_2O_5 loss pathways fractions calculated from steady state model and ambient temperature in (a) PKU2017 winter campaign and (b) TZ2018 summer campaign.

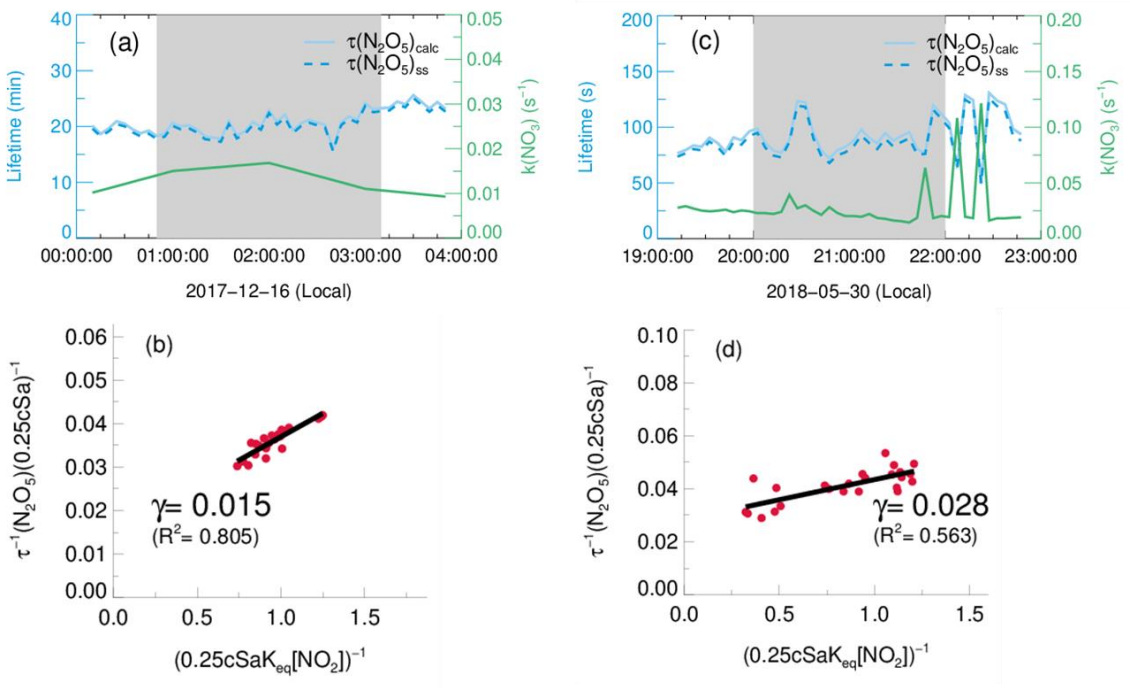

Figure S3. Example analysis of N_2O_5 lifetime and $\gamma_{ss}(N_2O_5)$ derivation through steady state fitting for (a)&(b) PKU2017 case in winter and (c)&(d) TZ2018 case in summer. The steady state lifetime and calculated atmospheric lifetime are shown as blue dash line and full line respectively. The green line is lumped NO_3 loss frequency. The red dots in (b)&(d) represent data points in the shadow area, used for steady state fit (black line) by the plot of $\left(0.25cS_a\tau_{ss}(N_2O_5)\right)^{-1}$ against $\left(0.25cS_aK_{eq}[NO_2]\right)^{-1}$. The text on the plot gives the best fit results of $\gamma_{ss}(N_2O_5)$ and correlation coefficient.

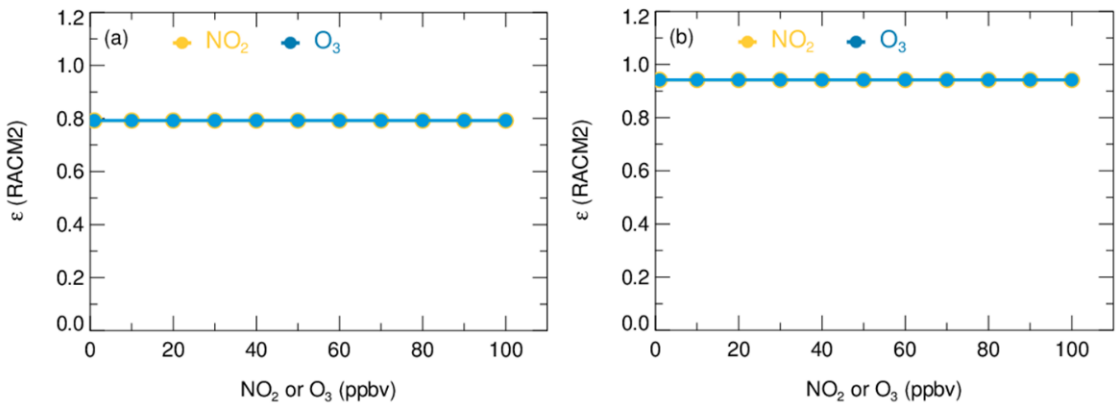

211

212 **Figure S4.** Sensitivity plot of NO_2 and O_3 concentration against coefficient ε calculated based on rate constants
213 from RACM2. (a) Initial model constraint is according to winter condition of PKU2017; (b) Initial model
214 constraint is according to summer condition of TZ2018.

215

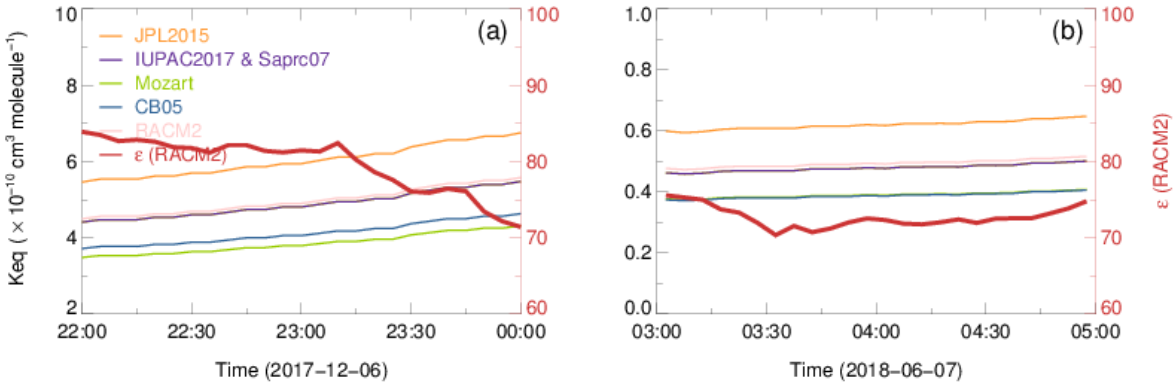

Figure S5. Exemplary comparison of *K*eq parameterization in (a) 2017-12-06 of PKU2017 dataset and (b) 2018-06-07 of TZ2018 dataset, using parameters from JPL2015 (orange), IUPAC2017&Saprc07 (purple), Mozart (green), CB05 (blue) and RACM2 (pink). It should be noted that the databases of Saprc07 and IUPAC2017 have the exactly same parameters, *K*eq derived from which are thus both denoted as purple line. The ε value calculated based on RACM2 is shown as red line.

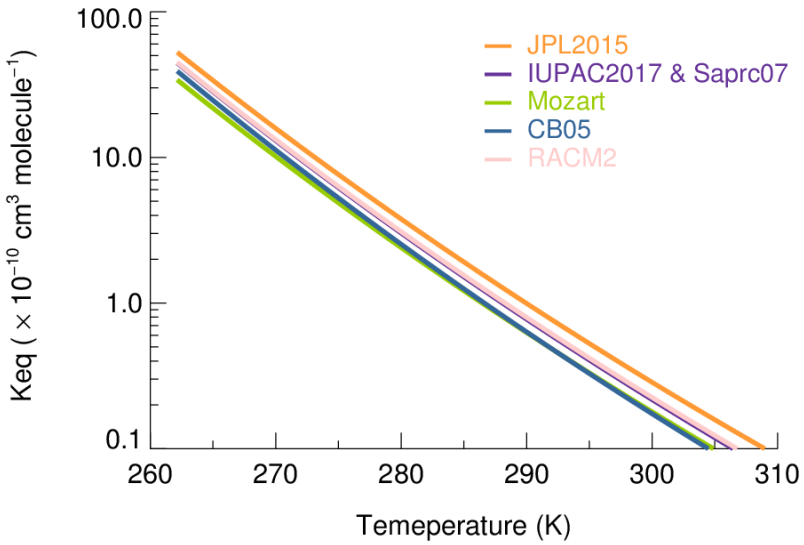

222

223 **Figure S6**. The dependence of different *K*eq parameterizations on temperature.

224

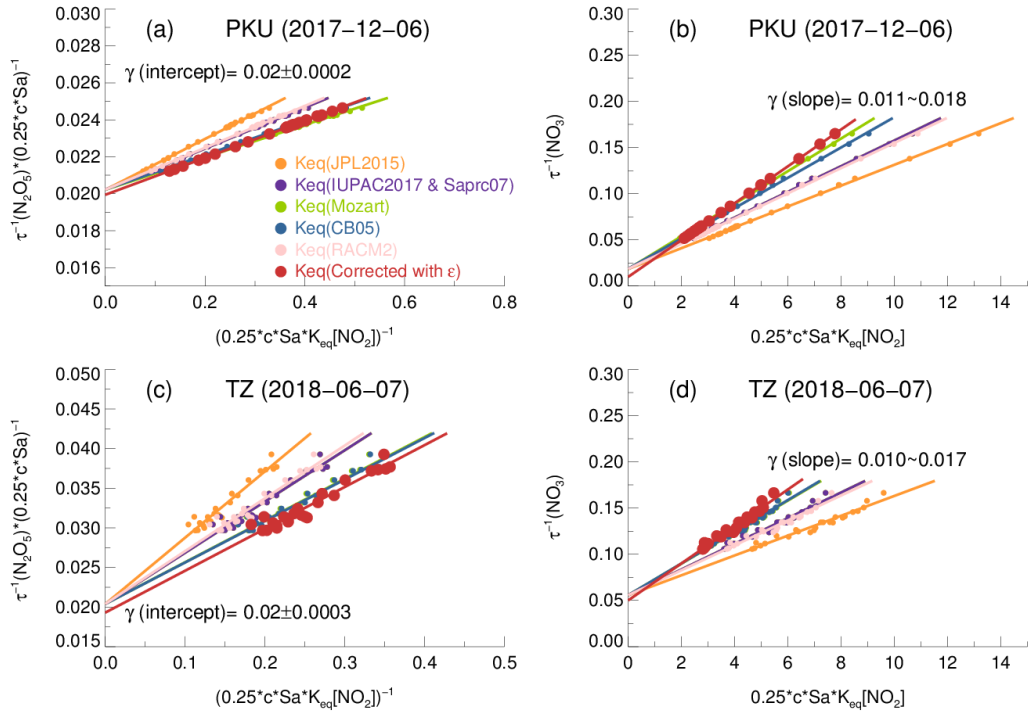

225

226 **Figure S7.** Exemplary fitting plot according to steady state approximation Eq. (1) (a)&(c) and Eq. (2) (b)&(d),
227 using *K*eq parameterization of JPL2015 (orange), IUPAC2017&Saprc07 (purple), Mozart (green), CB05 (blue)
228 and RACM2 (pink). The *K*eq (corrected by ε) is derived from output of steady state model coupled with RACM2.
229 The values of derived $\gamma(N_2O_5)$ by intercept or slope are shown in text in the figures.

230

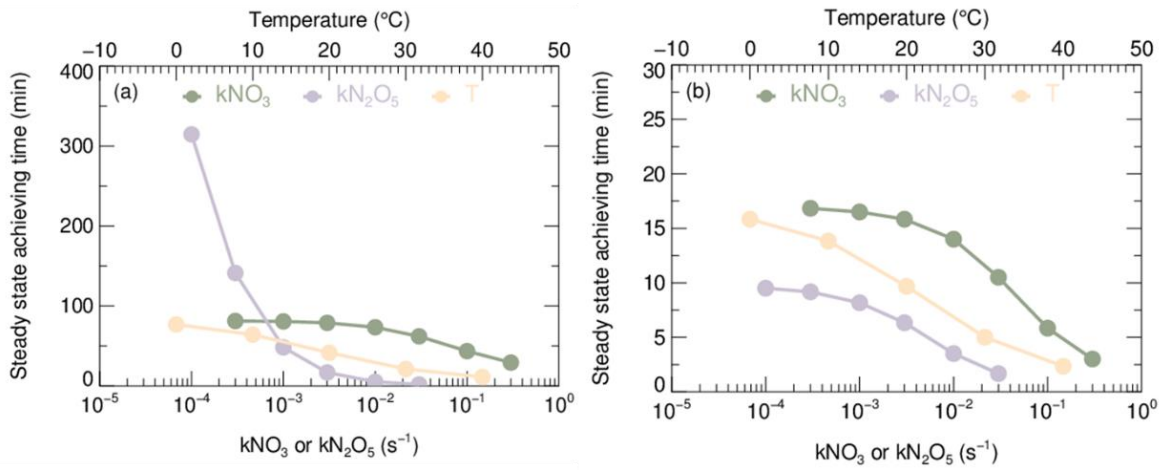

231

232 **Figure S8.** Sensitivity plot of $k$$NO_3$, $k$$N_2O_5$ and T against steady state achieving time of NO_3-N_2O_5 system. The
233 trace of T is plotted against the upper horizontal axis and the traces of the other two parameters are plotted
234 against the lower horizontal axis. (a) Initial model constraint is according to winter condition of PKU2017; (b)
235 Initial model constraint is according to summer condition of TZ2018.

236

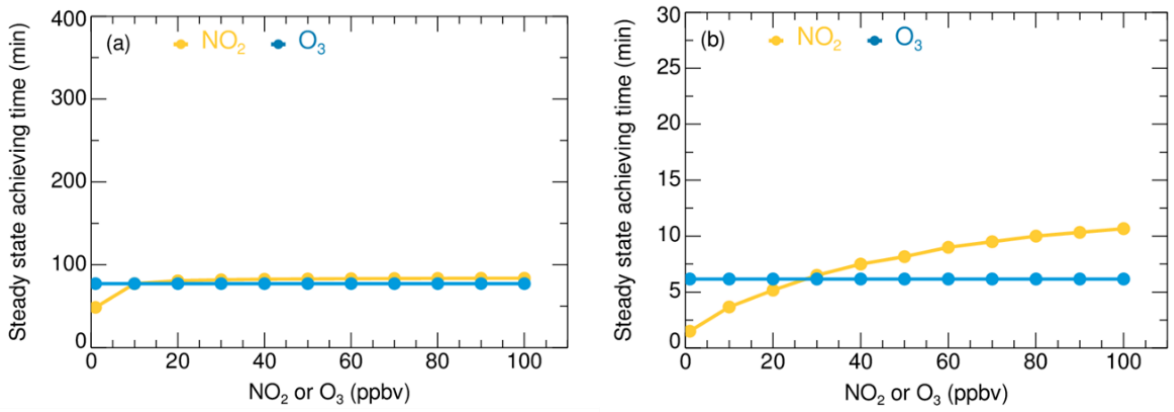

237

238 **Figure S9.** Sensitivity plot of NO_2 and O_3 concentration against steady state achieving time of NO_3-N_2O_5 system.
239 (a) Initial model constraint is according to winter condition of PKU2017; (b) Initial model constraint is according
240 to summer condition of TZ2018.

241

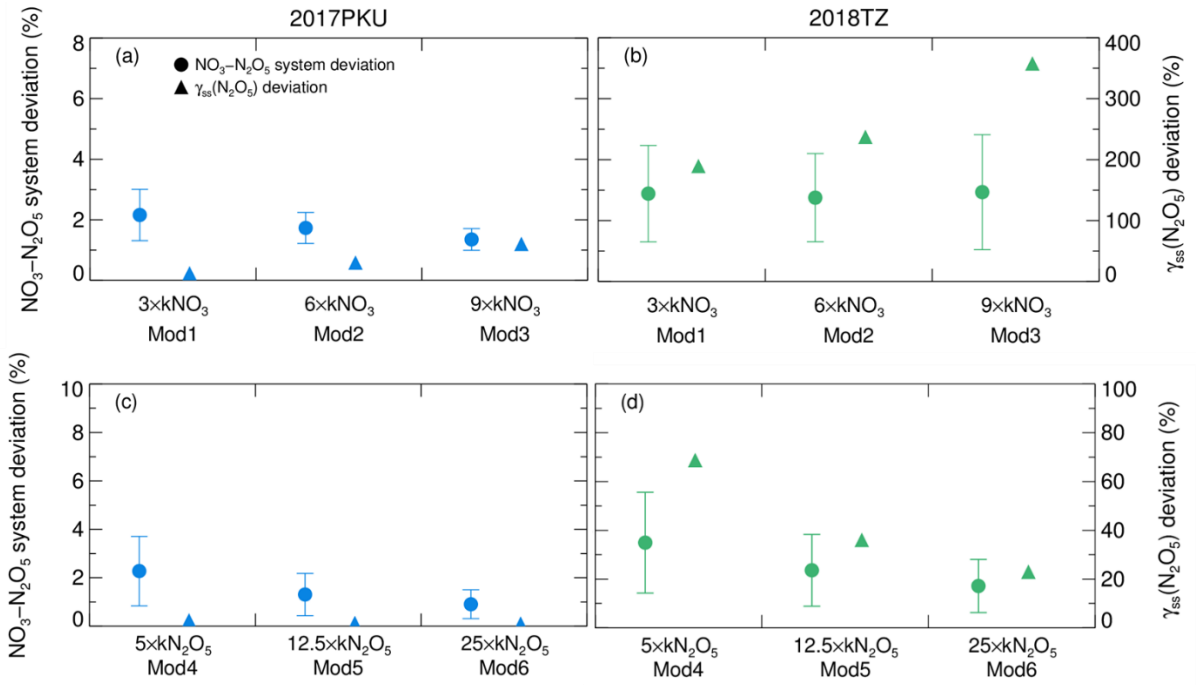

Figure S10. The average of NO_3-N_2O_5 system deviating from steady state and the median value of $\gamma_{ss}(N_2O_5)$ deviating from true value determined from different model constraints based on (a)&(c) PKU2017 dataset in blue and (b)&(d) TZ2018 dataset in green. The full circles represent the average of NO_3-N_2O_5 system deviating from steady state and the triangles represent the median deviation of $\gamma_{ss}(N_2O_5)$. As indicated in the text, the $k NO_3$ of Mod1, Mod2 and Mod3 are multiplied by 3,6 and 10 respectively against Mod0, and the $k N_2O_5$ of Mod4, Mod5 and Mod6 are multiplied by 5, 12.5 and 25 respectively against Mod0.

250 **Table S1.** Principal parameters and performance of related instruments.

Parameter	Technique	Time resolution	Detection Limit(1σ)	Accuracy
NO	Chemiluminescence[a]	1 min	200 pptv	±20%
NO_2	Chemiluminescence	1 min	300 pptv	±20%
O_3	UV photometry	1 min	500 pptv	±5%
VOCs	GC-MS/FID[b]	60 min	20-300 pptv	±15%
Monoterpene	PTR-MS[c]	10 s	20 ppyv	±15%
Sa	Nano SMPS, SMPS, APS	5 min	-	±10%

251 [a] Photolytic conversion to NO through blue light before detection; [b] Gas chromatography equipped with a mass spectrometer and a flame
252 ionization detector; [c] Monoterpene was only measured in TZ2018.
253

254 **Table S2.** Parameters of initial model constraint for sensitivity test.

Parameters	NO_2/ppbv	O_3/ppbv	T/K	Sa/$\mu m^2 \cdot cm^{-3}$	$\gamma(N_2O_5)$[a]	kNO_3/s^{-1}
Winter case	10	23	276	540	0.02	9×10^{-3}
Summer case	27	49	300	2670	0.02	9×10^{-2}

255 [a.] With the Sa, T and $\gamma(N_2O_5)$, the constraint of kN_2O_5 can be calculated as 6×10^{-4} s^{-1} for winter case and 3×10^{-3} s^{-1} for summer case.

256

Table S3. Summary of parameters for calculating rate constant of $k_{R1a.}$

Source	k_0^{300}	n	k_∞^{300}	m	F	g
JPL2015	2.4×10^{-30}	3.0	1.6×10^{-12}	-0.1	0.6	1.0
Mozart	2.0×10^{-30}	4.4	1.4×10^{-12}	0.7	0.6	1.0
CB05	2.0×10^{-30}	4.4	1.4×10^{-12}	0.7	0.6	1.0
Saprc07	3.6×10^{-30}	4.1	1.9×10^{-12}	-0.2	0.35	$0.75\text{-}1.27\times\log_{10}0.35$
RACM2	2.0×10^{-30}	4.4	1.4×10^{-12}	0.7	0.6	1.0
IUPAC2017	3.6×10^{-30}	4.1	1.9×10^{-12}	-0.2	0.35	$0.75\text{-}1.27\times\log_{10}0.35$

Table S4. Summary of parameters for calculating rate constant of k_{R1b}.

Source	k_0^{300}	n	k_∞^{300}	m	F	g	A	B_1	B_2
JPL2015 [a]	2.4×10^{-30}	3.0	1.6×10^{-12}	-0.1	0.6	1.0	5.8×10^{-27}	10840	10840
Mozart	2.2×10^{-30}	4.4	1.4×10^{-12}	0.7	0.6	1.0	3.0×10^{-27}	10900	10900
CB05 [b]	k_0^{300}/A= 1.0×10^{-3}	3.5	k_∞^{300}/A= 9.7×10^{14}	-0.1	0.45	1.0	-	11000	11080
Saprc07 [b]	k_0^{300}/A= 1.3×10^{-3}	3.5	k_∞^{300}/A= 9.7×10^{14}	-0.1	0.35	0.75-$1.27\times\log_{10}0.35$	-	11000	11080
RACM2	2.2×10^{-30}	4.4	1.4×10^{-12}	0.7	0.6	1.0	2.7×10^{-27}	11000	11000
IUPAC2017 [b]	k_0^{300}/A= 1.3×10^{-3}	3.5	k_∞^{300}/A= 9.7×10^{14}	-0.1	0.35	0.75-$1.27\times\log_{10}0.35$	-	11000	11080

a. This rate constant expression is reformed from k_{R1a}/Keq as defined in JPL2015, where the k_{R1a} and Keq are calculated with values recommended by JPL2015;

b. The k_0^{300}/A and k_∞^{300}/A are given in the form of ratio instead of separately.

References:

Brown, S. S., Stark, H., and Ravishankara, A. R.: Applicability of the steady state approximation to the interpretation of atmospheric observations of NO3 and N2O5, J. Geophys. Res.- Atmos., 108, 10.1029/2003jd003407, 2003.

Brown, S. S., Ryerson, T. B., Wollny, A. G., Brock, C. A., Peltier, R., Sullivan, A. P., Weber, R. J., Dube, W. P., Trainer, M., Meagher, J. F., Fehsenfeld, F. C., and Ravishankara, A. R.: Variability in nocturnal nitrogen oxide processing and its role in regional air quality, Science, 311, 67-70, 10.1126/science.1120120, 2006.

Brown, S. S., Dube, W. P., Fuchs, H., Ryerson, T. B., Wollny, A. G., Brock, C. A., Bahreini, R., Middlebrook, A. M., Neuman, J. A., Atlas, E., Roberts, J. M., Osthoff, H. D., Trainer, M., Fehsenfeld, F. C., and Ravishankara, A. R.: Reactive uptake coefficients for N2O5 determined from aircraft measurements during the Second Texas Air Quality Study: Comparison to current model parameterizations, J. Geophys. Res.- Atmos., 114, D00F10(01-16), Artn D00f10

10.1029/2008jd011679, 2009.

Cantrell, C., Davidson, J., McDaniel, A., Shetter, R., and Calvert, J.: The equilibrium constant for N2O5 = NO2 + NO3 - Absolute determination by direct measurement from 243 to 397 K, The Journal of Chemical Physics, 88, 10.1063/1.454679, 1988.

Cantrell, C., Shetter, R., Calvert, J., Tyndall, G., and Orlando, J.: Measurement of rate coefficients for the unimolecular decomposition of N2O5, The Journal of Physical Chemistry, 97, 10.1021/j100138a013, 1993.

Chang, W. L., Bhave, P. V., Brown, S. S., Riemer, N., Stutz, J., and Dabdub, D.: Heterogeneous Atmospheric Chemistry, Ambient Measurements, and Model Calculations of N2O5: A Review, Aerosol Sci. Technol., 45, 665-695, 10.1080/02786826.2010.551672, 2011.

Graham, R., and Johnston, H.: The photochemistry of the nitrate radical and the kinetics of the nitrogen pentoxide-ozone system, The Journal of Physical Chemistry, 82, 10.1021/j100492a002, 1978.

Kircher, C., Margitan, J., and Sander, S.: Pressure and temperature dependence of the reaction nitrogen dioxide + nitrogen trioxide + M .fwdarw. nitrogen pentoxide (N2O5) + M, The Journal of Physical Chemistry, 88, 10.1021/j150663a037, 1984.

Ma, X., Tan, Z., Lu, K., Yang, X., Liu, Y., Li, S., Li, X., Chen, S., Novelli, A., Cho, C., Zeng, L., Wahner, A., and Zhang, Y.: Winter photochemistry in Beijing: Observation and model simulation of OH and HO2 radicals at an urban site, Sci. Total Environ., 685, 85-95, https://doi.org/10.1016/j.scitotenv.2019.05.329, 2019.

Morgan, W. T., Ouyang, B., Allan, J. D., Aruffo, E., Di Carlo, P., Kennedy, O. J., Lowe, D., Flynn, M. J., Rosenberg, P. D., Williams, P. I., Jones, R., McFiggans, G. B., and Coe, H.: Influence of aerosol chemical composition on N2O5 uptake: airborne regional measurements in northwestern Europe, Atmos. Chem. Phys., 15, 973-990, 10.5194/acp-15-973-2015, 2015.

Osthoff, H., Pilling, M., Ravishankara, A. R., and Brown, S.: Temperature Dependence of the NO3 Absorption Cross-section Above 298 K and Determination of the Equilibrium Constant for NO3 + NO2 N2O5 at Atmospherically Relevant Conditions, Physical chemistry chemical physics : PCCP, 9, 5785-5793, 10.1039/B709193A, 2007.

Pritchard, H.: The nitrogen pentoxide dissociation equilibrium, Int. J. Chem. Kinet., 26, 61-71, 10.1002/kin.550260108, 1994.

Smith, C., and Ravishankara, A. R.: Kinetics of the reaction nitrogen dioxide + nitrogen trioxide + M at low pressures and 298 K, The Journal of Physical Chemistry, 89, 10.1021/j100254a024, 1985.

306 Wang, H., Chen, X., Lu, K., Tan, Z., Ma, X., Wu, Z., Li, X., Liu, Y., Shang, D., Wu, Y., Zeng, L., Hu, M., Schmitt,
307 S., Kiendler-Scharr, A., Wahner, A., and Zhang, Y.: Wintertime N2O5 uptake coefficients over the North China
308 Plain, Science Bulletin, 65, 765-774, https://doi.org/10.1016/j.scib.2020.02.006, 2020.
309